

# Geometrical Correction for the Inter- and Intramolecular Basis Set Superposition Error in Periodic Density Functional Theory Calculations

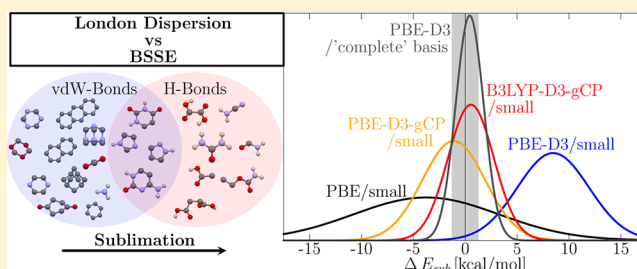
Jan Gerit Brandenburg,<sup>†</sup> Maristella Alessio,<sup>‡,¶</sup> Bartolomeo Civalleri,<sup>‡</sup> Michael F. Peintinger,<sup>†</sup> Thomas Bredow,<sup>†</sup> and Stefan Grimme<sup>\*,†</sup>

<sup>†</sup>Mulliken Center for Theoretical Chemistry, Institut für Physikalische und Theoretische Chemie der Universität Bonn, Beringstraße 4, 53115 Bonn, Germany

<sup>‡</sup>Department of Chemistry and Centre of Excellence NIS, University of Turin, Via P. Giuria 7, 10125 Torino, Italy

## Supporting Information

**ABSTRACT:** We extend the previously developed geometrical correction for the inter- and intramolecular basis set superposition error (gCP) to periodic density functional theory (DFT) calculations. We report gCP results compared to those from the standard Boys–Bernardi counterpoise correction scheme and large basis set calculations. The applicability of the method to molecular crystals as the main target is tested for the benchmark set X23. It consists of 23 noncovalently bound crystals as introduced by Johnson et al. (*J. Chem. Phys.* **2012**, *137*, 054103) and refined by Tkatchenko et al. (*J. Chem. Phys.* **2013**, *139*, 024705). In order to accurately describe long-range electron correlation effects, we use the standard atom-pairwise dispersion correction scheme DFT-D3. We show that a combination of DFT energies with small atom-centered basis sets, the D3 dispersion correction, and the gCP correction can accurately describe van der Waals and hydrogen-bonded crystals. Mean absolute deviations of the X23 sublimation energies can be reduced by more than 70% and 80% for the standard functionals PBE and B3LYP, respectively, to small residual mean absolute deviations of about 2 kcal/mol (corresponding to 13% of the average sublimation energy). As a further test, we compute the interlayer interaction of graphite for varying distances and obtain a good equilibrium distance and interaction energy of 6.75 Å and −43.0 meV/atom at the PBE-D3-gCP/SVP level. We fit the gCP scheme for a recently developed pob-TZVP solid-state basis set and obtain reasonable results for the X23 benchmark set and the potential energy curve for water adsorption on a nickel (110) surface.



## INTRODUCTION

The theoretical description of periodic systems using density functional theory (DFT) or Hartree–Fock (HF) with moderate computational costs is highly desirable. Especially the computation of reliable sublimation energies, geometries, and relative energies of molecular crystals and their polymorphic forms is of utmost importance, that is, aiming at crystal structure prediction.<sup>1–3</sup> The theoretical evaluation of molecular crystals and their polymorphs is an active research field.<sup>4–10</sup>

Bulk metals have a strongly delocalized valence electron density, and therefore, originless plane-wave-based basis sets are probably the best choice in orbital-based methods.<sup>11</sup> In molecular crystals, on the other hand, the charge density is more localized. Thus, for plane-wave-based methods, huge basis sets are needed. We have recently found that for a typical system of stacked organic  $\pi$ -systems, up to  $1.5 \times 10^5$  projector augmented plane-wave (PAW) basis functions must be considered for accurate results.<sup>12</sup> For this and similar systems, atom-centered basis functions could be much more efficient.<sup>13–16</sup>

Small atom-centered basis sets strongly suffer from basis set errors (BSEs), especially the basis set superposition error (BSSE). For molecular systems, a number of different correction schemes exist. Reference 17 gives a good review of the various approaches. Recently, we have mapped the standard Boys–Bernardi counterpoise correction (BB-CP) onto a semiempirical atom-pairwise potential.<sup>18</sup> This repulsive potential was fitted for a number of typical basis sets and depends only on the system geometry and was therefore denoted as geometrical counterpoise correction (gCP). Analytic gradients are problematic in nearly all other counterpoise schemes but are easily and efficiently obtained within the gCP. Moreover, the accidental error cancellation in standard small basis set calculations was recently demonstrated for molecular thermochemistry, and results could be significantly improved by applying gCP.<sup>19</sup>

In this work, we include periodic boundary conditions PBCs and unit cell gradients in the gCP code. We correct the

Received: July 5, 2013

Published: August 15, 2013

(semi)local density functionals for missing long-range electron correlation, also known as van der Waals or London dispersion interaction, with the DFT-D3 method.<sup>20</sup> The theory of both correction schemes, D3 and gCP, is briefly discussed. The proposed approach could also be applied analogously to HF calculations, but we restrict ourselves to DFT in this work. Computational details are summarized, and a short comparison of gCP and BB-CP energies is given. We test the applicability of the DFT-D3-gCP (or “functional”-D3-gCP) denoted method on the X23 benchmark set<sup>21,22,23</sup> for noncovalent interactions in molecular crystals and for the interaction between graphite layers. Furthermore, gCP parameters are calculated for a new solid-state optimized basis (pob-TZVP) and tested on the X23 sublimation energies, the graphite stacking, and for water adsorption on a nickel (110) surface. Finally, we give a conclusion.

## THEORY

We split the BSE into the basis set incompleteness error (BSIE) and BSSE. The BSIE arises always when finite incomplete basis sets are used. The BSSE is due to an inhomogeneous basis, that is, the variational freedom varies in different spacial regions. In the description of periodic systems, two types of single-particle basis sets are the most prominent, (1) a superposition of orthonormal plane-waves spread uniformly in space that is BSSE-free and (2) a direct product of a superposition of atom-centered functions and a momentum ( $\mathbf{k}$ )-dependent phase factor enforcing the correct translational symmetry. The atom-centered orbitals are typically contracted from primitive Gaussian functions with different exponents to decrease the computational effort. In the dissociation limit, each atom can be accurately described by this set. It is possible to choose the “most important” atom-centered basis functions and to minimize the BSIE with a fixed number of basis functions. Moreover, the use of Gaussian basis sets presents some advantages; core electrons can be easily treated, the algorithms are similar to those used in efficient molecular quantum chemistry codes where Gaussian orbitals are generally adopted, and the quasi-local character of electronic structure (at least for insulators) is more naturally exploited. However, incomplete, atom-centered basis sets always favor certain spatial locations.

Two major manifestations of the BSSE arise: (1) In the calculation of cohesive energies, the presence of surrounding molecules increases the basis relative to that in the dissociation limit, leading to an artificial overbinding; (2) in geometry optimizations, the atomic centers move, and therefore, the basis changes too. Unit cell volumes are artificially underestimated. A complete basis set is BSE-free; therefore, the best way to avoid both BSIE and BSSE is to increase the basis set, and this is always recommended if technically possible.

Unfortunately, in most periodic systems, large atom-centered basis sets are not commonly affordable. This is particularly relevant when diffuse functions with small Gaussian exponents are included. While they are important to describe the tails of molecular density distributions, they are less needed in periodic systems because the overlap between Bloch functions is higher than that between AOs in finite systems. Diffuse functions may lead to quasi-linear basis set dependencies that can cause an instability in the convergence of the iterative solution of the Kohn–Sham or HF equations (SCF procedure). Practically, it turns out to be difficult to enlarge the basis to the quadruple- $\zeta$  level, even in not very dense solids, although polarized triple- and quadruple- $\zeta$  basis sets have been employed occasionally in

calculations on molecular crystals.<sup>6,24–26</sup> Recently, a consistent triple- $\zeta$  basis set for periodic systems was developed by some of us, which aims to overcome some of the mentioned problems.<sup>27</sup> Therein, basis functions with very small exponents are consistently replaced by more localized contracted orbitals. However, we show below that the BSSE of this basis is still very large for typical cases and must be corrected.

Another problem of HF and common (semilocal) DFT functionals is that they are not capable of describing long-range electron correlation, that is, the London dispersion interaction. In order to get physically reasonable results, the methods have to be properly dispersion-corrected.<sup>28</sup> We decompose the total energy  $E_{\text{tot}}$  of a system into the DFT/HF energy  $E_{\text{DFT/HF}}$ , dispersion energy  $E_{\text{disp}}$ , and additional counterpoise correction  $E_{\text{gCP}}$

$$E_{\text{tot}} = E_{\text{DFT/HF}} + E_{\text{disp}} + E_{\text{gCP}} \quad (1)$$

To accurately describe the London dispersion interaction, we use our latest semiclassical ab initio dispersion correction DFT-D3.<sup>20,29</sup> It incorporates nonempirical, pairwise-specific, chemical environment-dependent dispersion coefficients, a physically sound damping function according to Becke and Johnson,<sup>30</sup> and optionally a nonadditive Axilrod–Teller–Muto three-body dispersion term.<sup>31</sup> The dispersion energy can be split into two- and three-body contributions  $E_{\text{disp}} = E^{(2)} + E^{(3)}$

$$E^{(2)} = -\frac{1}{2} \sum_{n=6,8} \sum_{A \neq B}^{\text{atom pairs}} \sum_{\mathbf{T}} s_n \frac{C_n^{AB}}{\|\mathbf{r}_B - \mathbf{r}_A + \mathbf{T}\|^n + f(R_0^{AB})^n} \quad (2)$$

$$E^{(3)} = -\frac{1}{6} \sum_{A \neq B \neq C}^{\text{atom triples}} \sum_{\mathbf{T}} \frac{C_9^{ABC} (3 \cos \theta_a \cos \theta_b \cos \theta_c + 1)}{r_{ABC}^9 \cdot (1 + 6(r_{ABC}/R_0)^{-\alpha})} \quad (3)$$

Here,  $C_n^{AB}$  denotes the averaged (isotropic)  $n$ th-order dispersion coefficient for atom pair  $AB$ , and  $\mathbf{r}_{A/B}$  are their Cartesian positions. The real-space summation over all unit cells is done by considering all translation invariant vectors  $\mathbf{T}$  inside of a cutoff sphere. The scaling parameter  $s_6$  equals unity for the here-applied functionals and ensures the correct limit for large distances, and  $s_8$  is a functional-dependent scaling factor. The rational damping function  $f(R_0^{ab})$  is

$$f(R_0^{ab}) = a_1 R_0^{ab} + a_2 \quad R_0^{ab} = \sqrt{\frac{C_8^{ab}}{C_6^{ab}}} \quad (4)$$

The dispersion coefficients are obtained from first-principle calculations for molecular systems with time-dependent DFT and application of the Casimir–Polder relation.<sup>32</sup> The three parameters  $s_6$ ,  $a_1$ , and  $a_2$  are fitted for each functional (or HF) on a benchmark set of small, noncovalently bound molecules. The fitting is necessary to prevent double counting of dispersion interactions at short range and to adjust repulsive and attractive parts. This procedure has an impact on the short- to medium-ranged part of the dispersion energy but does not affect the long-range regime, which is most important for periodic systems. In the three-body contribution,  $r_{ABC}$  corresponds to an averaged distance between the three pairs, and  $\theta_{a/b/c}$  are the corresponding angles. The general applicability of this atom-pairwise dispersion correction was shown in a number of recent publications by us<sup>33–35</sup> and other groups<sup>8,36,37</sup> and also for solids.<sup>12,38–41</sup> The importance of three- and many-body dispersion effects is currently not clear, but this question is intensively investigated.<sup>35,42,43</sup>

The most frequently used method to correct for the BSSE is the BB-CP<sup>44</sup> method. For a dimer AB with basis functions  $a$  and  $b$ , respectively, it reads

$$E_{\text{BB-CP}} = \{E(A)_a - E(A)_{ab}\} + \{E(B)_b - E(B)_{ab}\} \quad (5)$$

where  $E(A)_a$  is the energy of fragment A with basis functions  $a$  and  $E(A)_{ab}$  denotes the energy of the same fragment A with the enlarged basis  $ab$ . In the geometric counterpoise correction scheme, we map the BB-CP onto a semiempirical, repulsive pair potential  $V_A(r)$ , which decays exponentially with the interatomic distance  $r$

$$V_A(r) = e_A^{\text{miss}} \frac{\exp(-\alpha \cdot r^\beta)}{\sqrt{S \cdot N_B^{\text{virt}}}} \quad (6)$$

The energy difference between a large and the generally smaller target basis set for an atom A inside of a weak electric field  $e_A^{\text{miss}}$  is computed for all atoms. This quantity measures the incompleteness of the atomic target basis. The potential is normalized by the Slater overlap  $S$ , the number of virtual orbitals  $N_B^{\text{virt}}$ , and the empirical parameters  $\alpha$  and  $\beta$ . The Slater exponents of s- and p-valence orbitals  $\zeta_s$  and  $\zeta_p$ , respectively, are averaged to get a single s-function exponent  $\zeta_s^*$

$$\zeta_s^* = \eta \frac{\zeta_s + \zeta_p}{2} \quad (7)$$

with fit parameter  $\eta$ . In order to satisfy the PBCs, the summation runs over all distinct pairs AB inside of a large supercell of certain radius. Using a real-space cutoff is possible because of the exponential decay, which converges rapidly with increasing distance. We sum over all atom pairs and get the energy  $E_{\text{gCP}}$

$$E_{\text{gCP}} = \frac{\sigma}{2} \sum_{A \neq B}^{\text{atom pairs}} \sum_{\mathbf{T}} V_A(\|\mathbf{r}_A - \mathbf{r}_B + \mathbf{T}\|) \quad (8)$$

with a global scaling parameter  $\sigma$ .

Altogether, gCP involves four fit parameters ( $\sigma$ ,  $\alpha$ ,  $\beta$ ,  $\eta$ ) for each basis set. They have been fitted to reproduce the BB-CP energy of the large  $S66 \times 8$  noncovalent interaction benchmark set<sup>45</sup> by minimizing the root-mean-square deviation (RMSD). No parameter refit is considered here nor needed here for the applied standard basis sets (the new pob-TZVP basis<sup>27</sup> is discussed separately) because a short-range potential should not be affected by PBC. Parameters are available for a variety of basis sets, namely, the Ahlrichs-type basis sets SV, def2-SVP, and def2-TZVP,<sup>46–48</sup> the minimal basis set MINIS,<sup>49,50</sup> and the Pople-style basis 6-31G\*.<sup>51</sup>

## ■ COMPUTATIONAL DETAILS

We calculate the HF and DFT energies mostly with the widely used crystalline-orbital program CRYSTAL09.<sup>52,53</sup> In the CRYSTAL code, the Bloch functions are obtained by a direct product of a superposition of atom-centered Gaussian functions and a  $\mathbf{k}$ -dependent phase factor. We use the generalized gradient approximated (GGA) functional PBE<sup>54,55</sup> and the hybrid GGA functional B3LYP.<sup>56,57</sup> The  $\Gamma$ -centered  $\mathbf{k}$ -point grid is generated via the Monkhorst–Pack scheme<sup>58</sup> with 1  $\mathbf{k}$ -point for molecular calculations, 4  $\mathbf{k}$ -points for molecular crystals, and 12  $\mathbf{k}$ -points in each direction for graphite. The large integration grid (LGRID) and tight tolerances for Coulomb and exchange sums are used. The self-consistent field (SCF) energy threshold is set to  $10^{-8}$  Hartree. We exploit the polarized and unpolarized

split-valence basis set SVP and SV and the triple- $\zeta$  basis set pob-TZVP. Calculations close to the complete basis set limit (CBS) are carried out with the Vienna ab initio simulation package VASP 5.3.<sup>59,60</sup> We utilize the GGA functional PBE in combination with a PAW<sup>61,62</sup> with a huge energy cutoff of 1000 eV. This corresponds to  $\sim 200\%$  of the recommended high-precision cutoff and should accurately approximate the CBS for the here-investigated properties (denoted as PBE/CBS in the following).

We include the dispersion energy with the *dftd3* program in the Becke–Johnson damping scheme and a conservative distance cutoff radius of 95 Bohr. The BSSE correction is added via the gCP method as discussed above, where a smaller cutoff radius of 60 Bohr is used. Compared to the computation of the HF or DFT energies and gradients, the dispersion and counterpoise contributions require practically no additional computation time (even in a small basis, the HF or DFT calculation is 1–2 orders of magnitude slower).

The gCP correction will be also compared with the BB-CP scheme. In CRYSTAL, the BB-CP method is applied by supplementing the basis set of a single molecule, as cut out from the crystal structure, with the functions of an increasing number of atoms (ghost atoms) belonging to the surrounding array of molecules within a sphere of a given radius. Here, a sphere of 4.0 Å from each atom of the molecule is used. Tests with a larger radius of the sphere show a change of the lattice energies by only a few tenths of a kcal/mol.

For the geometry optimization, we use an extended version of the approximate normal coordinate rational function optimization program (ANCOPT).<sup>63</sup> The Cartesian coordinates of all atoms in one unit cell are transformed into approximate normal coordinates. In order to obtain reasonable internal coordinates, we translate all atoms by multiples of unit cell vectors in such a way that all molecular fragments are directly connected. We use a rational function algorithm to calculate the new coordinates from analytic atomic gradients and an interpolated Hessian matrix of second derivatives.<sup>64</sup>

Common unit cell optimizers rescale all atom positions inside of the unit cell to get the new coordinates. For molecular crystals, this procedure is very inefficient because all intramolecular distances change, and therefore, all atom gradients rise significantly. We perform a slightly different cell step. We identify all molecular fragments, calculate their center of mass, and transform all of these centers according to the new cell matrix. This keeps the intramolecular distances fixed, and we need fewer optimization steps. Full convergence is achieved if the energy change is below  $10^{-6}$  Hartree and if the gradient thresholds for the total atomic gradient ( $10^{-4}$  Hartree/Bohr) and total cell gradient ( $10^{-3}$  Hartree/Bohr) are fulfilled.

## ■ COMPARISON OF COUNTERPOISE CORRECTIONS

We first compare the gCP and BB-CP correction schemes with a large basis set calculation. We start this comparison by calculating potential energy curves for two simple cubic molecular crystals, namely,  $N_2$  and  $NH_3$ , with the hybrid functional B3LYP and small (SVP) and large (QZVP<sup>65</sup>) basis sets. By starting from the experimental crystal structures, the lattice parameter has been varied in a range of  $-10 < a < +15\%$  by fixing the internal coordinates of the molecules at their experimental values. In Figure 2, the gCP corrected potential energy curves are shown. In the case of  $N_2$ , the curve obtained with the small basis set shows a minimum not far from the experimental lattice constant of 5.649 Å, while the BB-CP

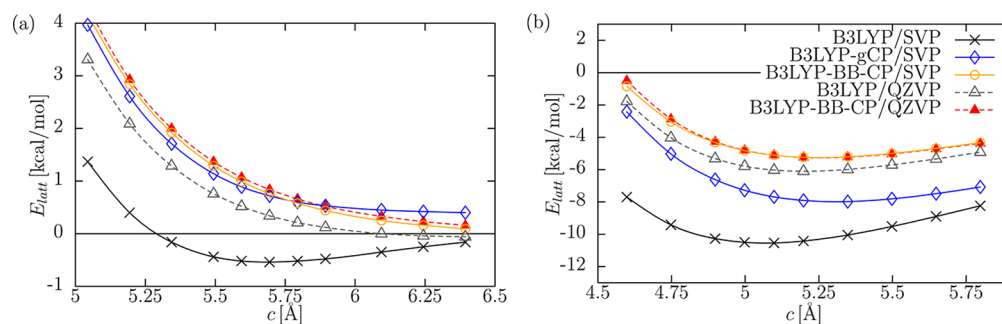


**Figure 1.** Potential energy curves for (a)  $\text{N}_2$  and (b)  $\text{NH}_3$  molecular crystals. The lattice parameter is changed around the experimental value. The B3LYP/SVP curves that include either the gCP or the BB-CP corrections are compared with the B3LYP/QZVP one (with and without BB-CP correction).

corrected one is purely repulsive. This is expected because of the very weak dispersion-dominated intermolecular interactions in solid  $\text{N}_2$  and the well-known failure of the B3LYP functional in properly describing van der Waals interactions. The artificial minimum is evidently due to the BSSE, as confirmed by the results with the larger QZVP basis set, which shows only a very small BSSE. The gCP correction removes most of the BSSE and closely reproduces the BB-CP corrected curve. A closer inspection shows that the gCP approach gives a better agreement with BB-CP at shorter lattice parameters, while it overestimates the correction when the cell is expanded. For ammonia (Figure 1b), similar results are found. However, the gCP corrected lattice energies tend to be underestimated with respect to the BB-CP ones. Larger deviations are observed as the lattice constant enlarges. Notably, for both molecular crystals, the B3LYP/QZVP results are still affected by some BSSE. This indicates that the utilized QZVP basis still suffers from incompleteness, which leads to a significant BSSE.

Additionally, we investigate the urea crystal in the same fashion. In order to have a single variable to scan, we adopt the following procedure. By starting from the experimental crystal geometry (tetragonal) as measured at 12 K by neutron powder diffraction,<sup>66</sup> the lattice energy is computed as a function of the lattice constant  $a$  while the lattice parameter  $c$  is varied by fixing the  $c/a$  ratio at its experimental value (i.e., 0.8417). We change the lattice parameter in a range between  $-5.4$  and  $+10.8\%$ . Expansion and contraction of the lattice parameters are carried out in a rigid body approach. This means that during the cell deformation, the internal geometry of the urea molecule is kept fixed. As can be seen in Figure 2, the crystal is bound on all theoretical levels. This is expected because of the strong

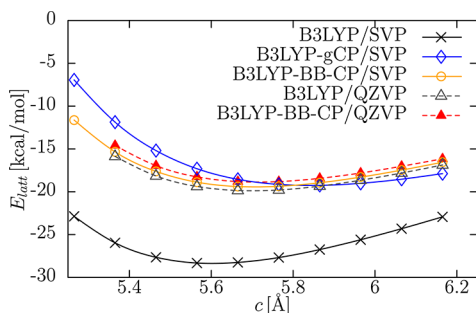


**Figure 2.** Potential energy curves for urea. The lattice parameter is changed around the experimental value. The B3LYP/SVP curves that include either the gCP or the BB-CP corrections are compared with the B3LYP/QZVP one (with and without BB-CP correction).

hydrogen bonds, which can be properly described by the (semi)local hybrid functional B3LYP. However, the binding energy is strongly overestimated by 42% on the B3LYP/SVP level compared to the B3LYP/QZVP result. We correct the small basis calculation with the standard BB-CP correction and with the new gCP scheme. Deviations of the binding energy compared to the B3LYP/QZVP level diminish to 2 and 3% on the B3LYP-BB-CP/SVP and B3LYP-gCP/SVP levels, respectively. As shown in Figure 2, the gCP curve is in good agreement with the BB-CP and the large QZVP basis set. While the gCP corrected energy is very close to the BB-CP corrected one, the minimum is slightly shifted to larger values. This will change the equilibrium in unconstrained geometry optimizations toward too large unit cells. We present a more detailed analysis and workaround in the following section.

Overall, in the three cases, the gCP approach appears to reasonably reproduce the BB-CP correction at least regarding the lattice energies. The shape of the potential energy profile is qualitatively corrected in the right direction, but we note a slight inconsistency between the crystal energy and geometry. This is important for geometry optimization, as will be discussed in the next section. Note that dispersion corrections have not been applied yet, which is mandatory when comparisons to experimental data are made, as discussed in the next section.

## ■ X23 BENCHMARK SET

A benchmark set for noncovalent interactions in solids consisting of 21 molecular crystals (dubbed C21) was compiled by Johnson<sup>21</sup> recently. Two data sets are considered, (1) thermodynamically back-corrected experimental sublimation energies and (2) structural data from low-temperature X-ray diffraction. The thermal and zero-point effects were explicitly accounted for. Therefore, we can directly compare the electronic energy differences with the back-corrected experimental values. The error bar of experimental sublimation energies was estimated to be 1.2 kcal/mol.<sup>67</sup> Recently, the C21 set was extended and refined by Tkatchenko et al.<sup>22</sup> The X23 benchmark set (16 systems are presented in ref 22 and 7 additional systems in ref 23) includes two additional molecular crystals, namely, hexamine and succinic acid. The molecular geometries of the X23 set are shown in Figure 3. The details of the back-correction procedure are summarized in ref 23. The mean absolute deviation (MAD) between both reference data sets is 0.55 kcal/mol. Because the X23 data seem to be more consistent, we use them here as reference. If we take the standard deviation (SD) between both thermodynamic

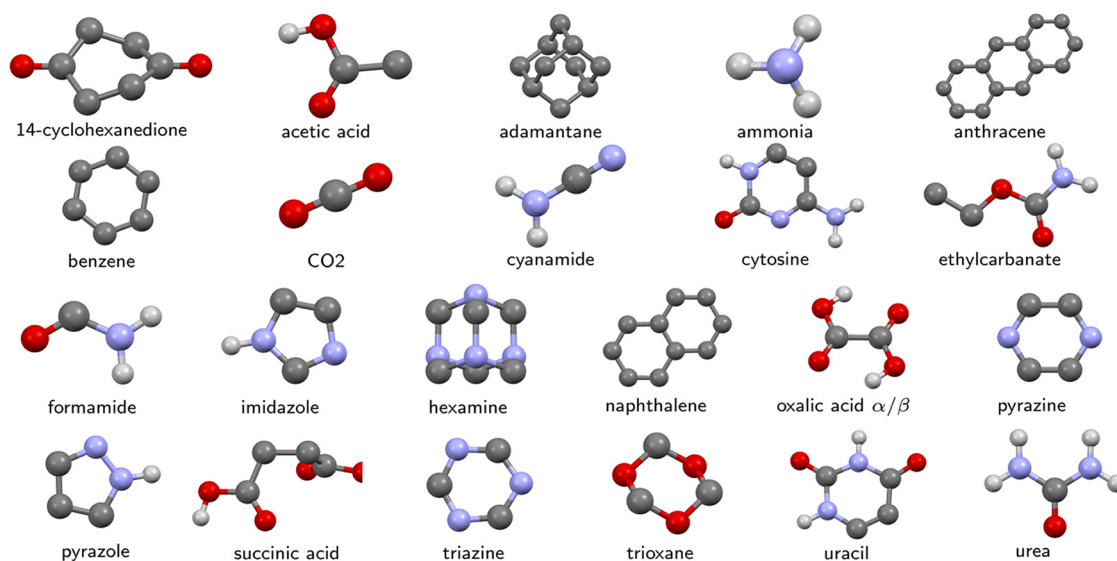


**Figure 3.** Geometries of the 23 small organic molecules from the X23 benchmark set for noncovalent interactions in solids. H atoms at carbons are omitted for clarity. Carbons are denoted by dark gray balls, hydrogens are light gray, oxygens are red, and nitrogens are light blue.

corrections as an independent error source, we can add the squared errors to the total uncertainty of the reference values and obtain about 1.3 kcal/mol as statistical error. We calculate sublimation energies and crystal geometries utilizing the GGA functional PBE and the hybrid GGA functional B3LYP with a small polarized split-valence basis set SVP. The PBE/CBS values are computed with the VASP program package. In the sublimation energy calculations, the isolated molecules are approximated by a large unit cell calculation with a minimum distance between molecule images of 16 Å. In order to calculate the sublimation energy, we optimize the isolated molecule and the corresponding molecular crystal. The unit cells are kept fixed at the experimental values. We summarize the deviations from reference data in Table 1. The individual values for all systems are given in the Supporting Information (SI). First, the

**Table 1. MAD, Mean Deviation (MD), and SD of the Sublimation Energy for the X23 Test Set and for the Subset X12/Hydrogen Dominated by Hydrogen Bonds<sup>a</sup>**

method	X23			X12/hydrogen	
	MAD	MD	SD	MAD	MD
PBE/CBS	11.7	-11.7	6.1	9.7	-9.7
PBE-D3/CBS	1.1	0.4	1.3	1.3	0.8
PBE-D3/CBS+E <sup>(3)</sup> <sup>b</sup>	1.2	-0.5	1.7	1.1	0.1
PBE/SVP	5.4	-3.8	7.0	2.6	-0.1
PBE-D3/SVP	8.5	8.5	3.5	10.5	10.5
PBE-D3-gCP/SVP	2.5	-1.1	3.0	2.8	-1.4
PBE-D3-gCP/SVP+E <sup>(3)</sup> <sup>b</sup>	2.9	-2.0	3.2	3.1	-2.2
B3LYP-D3/SVP	10.1	10.1	4.1	12.0	12.0
B3LYP-D3-gCP/SVP	2.0	0.6	2.2	1.7	-0.1
B3LYP-D3-gCP/SVP+E <sup>(3)</sup> <sup>b</sup>	1.7	-0.3	2.2	1.8	-0.8

<sup>a</sup>We calculate the energy with different combinations of functionals (PBE and B3LYP), dispersion correction D3, and geometric counterpoise correction gCP and compare with thermodynamically back-corrected experimental sublimation energies. On the PBE/SVP level, we give values based on deviations to the corresponding large plane-wave basis set values in the SI. All values are in kcal/mol. <sup>b</sup>Three-body dispersion single-point energy  $E^{(3)}$  on optimized structures.

exceptionally small MAD of 1.1 kcal/mol on the PBE-D3/CBS level should be mentioned, which is within the estimated experimental error. The importance of the D3 correction is obvious from the huge error of plain PBE/CBS, which very strongly underbinds most of the crystals. The D3 uncorrected functional (PBE/SVP) yields a smaller error than the corresponding CBS result, which is due to the BSSE. Because of the very encouraging results of the D3 scheme in the estimated CBS limit and the physical significance of dispersion in periodic systems, we will only report and discuss D3 corrected results in the following.

Without BSSE correction, the MADs are 8.5 and 10.1 kcal/mol on the PBE-D3/SVP and B3LYP-D3/SVP level, respectively. The mean deviation (MD) and the MAD are identical, meaning that the sublimation energy is artificially overestimated in all tested systems. Utilizing the gCP potential for BSSE correction, the MAD drops drastically to 2.5 and 2.0 kcal/mol, respectively, for the two methods. The BSSE corrected small basis set PBE-D3 results nicely match those at the estimated CBS limit obtained with the BSSE-free plane-wave basis. Figure 5 shows the correlation between the PBE-D3(-gCP)/SVP energies and the experimental reference values. The remaining BSE is of the same order of magnitude as the error of the corresponding CBS calculation. Additionally, we investigate the effect of three-body dispersion for all levels of theory. The correlation plot between the B3LYP-D3(-gCP)/SVP(+ $E^{(3)}$ ) energies and the reference values is shown in Figure 4. The three-body term is repulsive for all systems and significantly improves the results for the B3LYP functional (see Table 1). However, the PBE-D3 errors are slightly larger with the three-body term. The MAD is 1.7 and 1.2 kcal/mol, respectively, on the B3LYP-D3-gCP/SVP+E<sup>(3)</sup> and PBE-D3/CBS+E<sup>(3)</sup> level. Tentatively, this can be attributed to the very different many-body behaviors of the two functionals for overlapping densities, as noted already some years ago.<sup>68</sup>

We compute the deviations separately for hydrogen- and non-hydrogen-bonded systems to investigate the different energetic contributions. Results are also reported in Table 1. On the PBE-D3/CBS level, the sublimation energies of hydrogen-bonded systems (X12/hydrogen subset) are system-

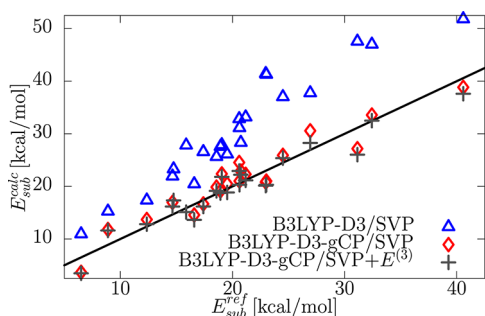


**Figure 4.** Sublimation energy per molecule for the X23 set on the B3LYP-D3/SVP, B3LYP-D3-gCP/SVP, and B3LYP-D3-gCP/SVP +  $E^{(3)}$  levels. We compare with thermodynamically back-corrected experimental energies  $E_{\text{sub}}^{\text{ref}}$ .

atically too large. The systematic overbinding of PBE for such systems is well-known from molecular complexes<sup>33,69</sup> and, not unexpectedly, transfers to molecular crystals. However, for the small SVP basis, the sublimation energies of the X12/hydrogen set are systematically underestimated by 2.2 and 0.8 kcal/mol on the PBE-D3-gCP/SVP +  $E^{(3)}$  and B3LYP-D3-gCP/SVP +  $E^{(3)}$  levels, respectively. We explain this underbinding by the lack of a second set of polarization functions with smaller exponents. This prevents the system from a proper polarization in an electric field, which is significant in hydrogen bonds. The effect is very dominant in both oxalic acid polymorphs and succinic acid and explains their larger error (visible in Figures 4 and 5).

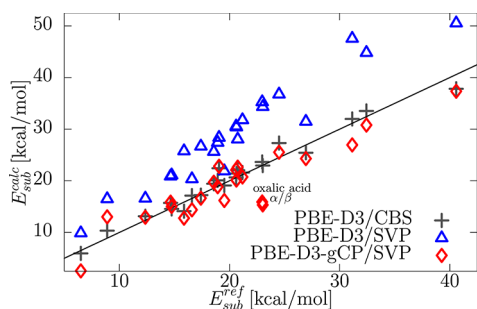


**Figure 5.** Sublimation energy per molecule for the X23 set on the PBE-D3/SVP and PBE-D3-gCP/SVP levels. We compare with thermodynamically back-corrected experimental energies. The energies are calculated on optimized structures with experimental lattice constants.

For both functionals,  $\alpha/\beta$ -oxalic acid have the largest deviation from the reference values. For  $\alpha$ -oxalic acid, the sublimation energy is overestimated with PBE-D3/CBS by 4.7 kcal/mol, while it is underestimated with PBE-D3-gCP/SVP +  $E^{(3)}$  and B3LYP-D3-gCP/SVP +  $E^{(3)}$  by 8.4 and 2.7 kcal/mol, respectively. The errors in describing hydrogen bonds with the PBE functional are significantly larger than those with the hybrid functional B3LYP.

For 11 crystals of the X23 set, we perform a full geometry optimization and explore the PBE functional. For eight systems, we additionally investigate the performance of the hybrid functional B3LYP. A more detailed analysis of these structural data is presented in the SI. As the most sensitive observable, we compare the unit cell volume with the experimental values in Table 2. Due to thermal length expansions, the calculated 0 K cell volumes should be smaller than the measured ones. Thermal expansions of these systems are estimated to be

**Table 2.** MAD and MD of the Unit Cell Volumes<sup>a</sup>

method	MAD	MD	rel. MD (%)
PBE-D3/CBS	4.2 (0.0)	-1.5 (0.0)	-0.8
PBE-D3	17.5 (15.9)	-17.5 (-15.9)	-6.1
PBE-D3-(1/2)gCP	7.5 (5.8)	-3.3 (4.9)	1.0
PBE-D3-gCP	23.7 (25.3)	23.7 (25.3)	7.9
B3LYP-D3	22.1	-22.1	-9.1
B3LYP-D3-(1/2)gCP	6.6	-6.6	-2.9

<sup>a</sup>We calculate the geometries with different combinations of functionals PBE and B3LYP with the SVP basis, dispersion correction D3, and geometric counterpoise correction gCP. Deviations with respect to the CBS values are given in parentheses. Absolute values are in  $\text{\AA}^3$ .

approximately 3%, while also larger thermal expansions up to 8% were reported.<sup>70</sup> The estimated PBE-D3/CBS results have a small MAD of 4  $\text{\AA}^3$ . As expected, the unit cells are systematically too small by 0.8%. With the SVP basis set, the BSSE artificially shrinks the crystal by, on average, 6% on the PBE-D3/SVP level. With the full counterpoise correction, we obtain unit cell volumes that are by 8% too large. The full BB-CP is known to overestimate the BSSE in large and dense systems.<sup>71</sup> While this seems not to be the case for the sublimation energies, we notice a significant effect on the crystal geometry, which, however, at present is not entirely clear. Empirically, it has been found before<sup>71-76</sup> that half of the counterpoise correction is a reasonable workaround. Indeed, when the gCP correction is reduced to 50%, a good agreement with the experimental data is obtained. The MAD drops from 17 to 7  $\text{\AA}^3$  on the PBE-D3/SVP and PBE-D3-(1/2)gCP/SVP levels, respectively. The MADs with respect to the corresponding PBE-D3/CBS values are smaller. This indicates that some of the remaining errors do not arise because of BSE but rather due to shortcomings of the PBE functional, as noted in the previous paragraph. The unit cell volume of the systems dominated by hydrogen bonds has a MD of 5  $\text{\AA}^3$  with respect to the CBS estimate, while the non-hydrogen-bonded systems have a significantly smaller MD of 2  $\text{\AA}^3$ . Again, in the description of hydrogen bonds, B3LYP performs better than PBE. In Figure 6, we show the correlation with the

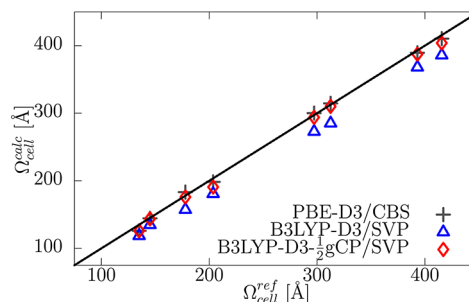


**Figure 6.** Unit cell volumes for eight representative crystals of the X23 set on the B3LYP-D3/SVP and B3LYP-D3-(1/2)gCP/SVP levels. We compare with experimental low-temperature X-ray data.

experimental unit cell volumes. Utilizing BSSE uncorrected B3LYP-D3/SVP, the unit cell volumes are underestimated by 9%, while with 50% of the gCP correction, very reasonable geometries, too small by only 3%, are obtained.

## GRAPHITE: INTERLAYER DISTANCE AND ENERGY

In order to demonstrate the applicability of the gCP correction for denser systems, we investigate the interactions between graphite layers. The experimental interlayer equilibrium distance is  $3.34 \pm 0.03 \text{ \AA}$ .<sup>77</sup> The experimental exfoliation energies have a large spread and range from  $-35$  to  $-52 \text{ meV}$  per atom.<sup>78–81</sup> We studied a similar system previously and demonstrated the applicability of the semiempirical dispersion correction DFT-D2.<sup>82,83</sup> The earlier study was done by an extrapolation of different finite size graphene layers. Significant errors were noted utilizing basis sets below the quadruple- $\zeta$  level.

Here, we describe the system periodically and investigate the effect of BSSE. For our calculations, we use the PBE functional with unpolarized split valence basis set SV. We compute the interlayer binding energy of graphite for different interlayer distances  $c$  (PES) shown in Figure 7. The plain PBE functional

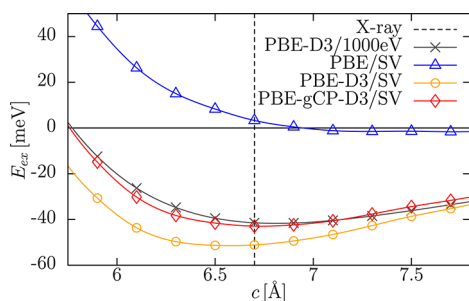


**Figure 7.** Exfoliation energy  $E_{\text{ex}}$  of two graphite layers per atom as a function of the stacking distance  $c$ . We explore the PBE functional with the SV basis and huge PAW (dubbed as CBS) basis sets. The vertical line denotes the experimental value. The cell parameters  $a$  and  $b$  are fixed to the experimental values.

shows no significant minimum in the potential energy curve, and no net bonding is observed. Adding the D3 correction, the minimum distance is underestimated by  $0.2 \text{ \AA}$  due to BSSE. At the gCP corrected level, a perfect agreement between theory and experiment is found. Calculations with huge BSSE-free plane-wave basis sets confirm the identified PBE-D3 minimum. Especially in the minimum region, the agreement between the PBE-D3-gCP/SVP and PBE-D3/CBS results is excellent. We calculate an exfoliation energy of  $-43.0 \text{ meV/atom}$  on the PBE-D3-gCP/SVP level. This is reasonable in comparison to the experimental estimates, and it differs by only 3% from the PBE-D3/CBS value.

We investigate the same system on the PBE/pob-TZVP level. The additional basis functions increase the BSSE significantly, resulting in an artificial minimum at an interlayer distance of  $3.2 \text{ \AA}$ . This seemingly good result arises from an accidental error cancellation. The BSSE gives an artificial attraction that simulates, near the minimum, the neglected dispersion attraction. However, the exponentially decaying BSSE cannot accurately mimic the dispersion interaction, which decays as  $r^{-6}$  with the interatomic distance for each atom pair. This is demonstrated in Figure 8, where we analyze the long-range behavior of the interlayer interaction on the PBE-D3-gCP/SV and PBE(-D3-gCP)/pob-TZVP levels. We fit a power law  $E_{\text{ex}} \propto c^{-n}$  in a least-squares sense for distances  $c$  in the interval of  $[10, 20] \text{ \AA}$ .

The combination of PBE/SV, D3, and gCP shows the correct asymptotic behavior of  $c^{-4}$  for insulating infinite layers. For the

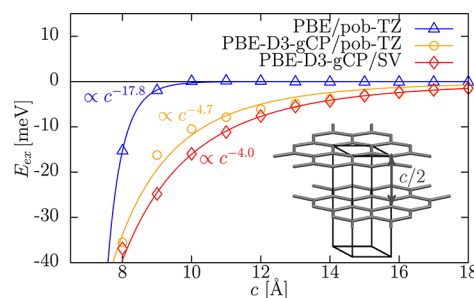


**Figure 8.** Exfoliation energy  $E_{\text{ex}}$  of two graphite layers per atom as a function of the stacking distance  $c$  in the long-range limit. The continuous lines correspond to a power law fit with critical exponents of 18 and 4 for the PBE/pob-TZVP and PBE-D3-gCP/SV levels, respectively. The cell parameters  $a$  and  $b$  are fixed to the experimental values.

special case of graphite ( $k$ -point conductor) the true dependence is  $c^{-3} \ln(c/c_0)$ .<sup>84</sup> We find a critical exponent of 4.03, which nicely agrees with the value of 4.2 as predicted by means of quantum Monte Carlo calculations.<sup>85</sup> On the other hand, the raw PBE functional with a triple- $\zeta$  basis exhibits a more exponential behavior (the exponent for the power-law fit is about 18), as expected.

## GCP CORRECTION FOR THE POB-TZVP BASIS

We mentioned the problem of near-linear dependencies that arise if basis functions with small exponents are included in periodic calculations of dense systems. Even with the Ahlrichs SVP basis set, we encounter some SCF convergence problems. Recently, a new Gaussian basis set, denoted as pob-TZVP, was developed,<sup>27</sup> which provided stable and robust SCF convergence for a wide range of solids. However, we demonstrated above that its BSSE can be huge. The main targets of these basis sets are bulk systems or surfaces where both dispersion interactions and BSSE artifacts are important. Therefore, we determined the gCP parameters for the pob-TZVP basis in the same way as described in the original ref 18 using the TURBOMOLE program suite.<sup>86</sup> We calculated the  $e^{\text{miss}}$  parameters for all elements H–Br (excluding rare gases) between the restricted open-shell HF energy  $E_{\text{ROHF}}$  for the target basis and a large quadruple- $\zeta$  basis def2-QZVPD according to

$$e^{\text{miss}} = E_{\text{ROHF}}^{\text{target basis}} - E_{\text{ROHF}}^{\text{large basis}}|_{F=0.06 \text{ au}} \quad (9)$$

where  $F = 0.06 \text{ au}$  denotes an applied weak electric field in order to populate higher angular momentum functions. These values can be used to judge the completeness of an atomic basis set, as discussed in the original gCP work. In this regard, the pob-TZVP and the SVP basis sets are rather similar, with mean  $e^{\text{miss}}$  parameters of 0.24 and 0.22 hartree, respectively. We fit the four parameters  $\sigma$ ,  $\alpha$ ,  $\beta$ , and  $\eta$  in eq 8 to computed BB-CP data at the B3LYP/pob-TZVP level for the  $S66 \times 8^45$  benchmark set. The optimized parameters are

$$\begin{aligned} \sigma &= 0.1300 & \alpha &= 1.3743 \\ \beta &= 0.4792 & \eta &= 1.3962. \end{aligned} \quad (10)$$

The RMSDs of the fit for the pob-TZVP and SVP basis sets are 0.002 and 0.001 hartree, respectively, that is, the Ahlrichs basis set SVP seems to be better balanced.

For the X23 benchmark set, presented previously, the MAD of the sublimation energies is significantly reduced from 10.7

kcal/mol on the PBE-D3/pob-TZVP level to 4.7 kcal/mol on the PBE-D3-gCP/pob-TZVP level. The asymptotic behavior of the interlayer interaction in graphite is also improved. The scaling exponent of 4.72 on the PBE-D3-gCP/pob-TZVP level represents a huge improvement compared to the unphysical value of 17.83 for plain PBE/pob-TZVP. Although the dispersion and BSSE corrected pob-TZVP basis set work reasonably well, we recommend using the Ahlrichs-type basis set for calculations on molecular crystals.

One of the most important applications of bulk-optimized basis sets in combination with correction schemes for dispersion and BSSE is the description of adsorption of molecules on surfaces. Neglecting even one of these effects can lead to significant errors. We therefore demonstrate the application of our periodic BSSE correction scheme for the adsorption of water on Ni(110) (see Figure 9). Water adsorbs

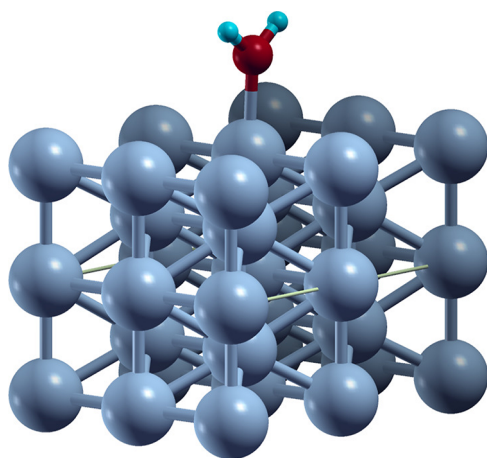


**Figure 9.** Model system for the adsorption of H<sub>2</sub>O on the Ni(110) surface.

oxygen down on the Ni(110) surface at a top position. The Ni–OH<sub>2</sub> distance was determined by surface-extended X-ray absorption fine structure (SEXAFS) spectroscopy to be  $2.06 \pm 0.03$  Å.<sup>87,88</sup>

The Ni bulk was optimized employing the PBE functional and the pob-TZVP basis set. With 3.451 Å for the unmodified pob basis set, the deviation from the experimental lattice constant<sup>89</sup> of 3.524 Å is only 2%. A  $2 \times 2$  supercell slab model ( $a = 4.881$  Å,  $b = 6.902$  Å) with five atomic layers was optimized, allowing full relaxation of all atoms. The structure of the water molecule was optimized in the gas phase, also employing the PBE functional and the pob-TZVP basis set, and set on top of a center Ni atom (see Figure 10).

We varied the Ni–OH<sub>2</sub> bond distance from 1.7 to 2.3 Å, fixing the orientation of the water molecule. Without any correction, PBE/pob-TZVP seems to give the correct value of 2.05 Å. When applying only the D3 correction, a slight overbinding (2.00 Å) is found, while applying only the gCP correction overestimates the bond distance (2.15 Å). Correcting for dispersion as well as for the BSSE, the Ni–OH<sub>2</sub> bond distance (2.05 Å) is in perfect agreement with that from experiment.

## CONCLUSIONS

We presented and evaluated the semiempirical gCP for use in periodic DFT calculations. The gCP correction is added to the total (ideally dispersion corrected) DFT energy and approx-

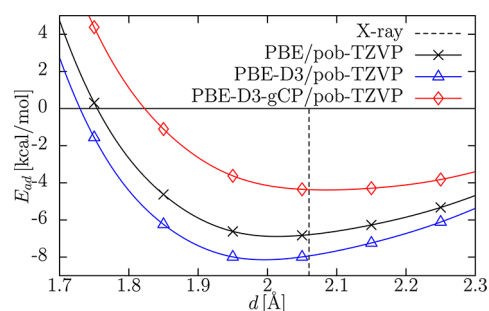


**Figure 10.** Potential energy surface of the water adsorption on a Ni(110) surface with varying Ni–OH<sub>2</sub> distance  $d$ . We utilize the PBE functional with the pob-TZVP basis set and explore the effects of D3 and gCP correction.

imates the Boys–Bernardi counterpoise energy in a fast and differentiable way for various atom-centered Gaussian basis sets. A benchmark set for noncovalent interactions in solids (X23) is exploited to evaluate the performance of various DFT methods also with small Gaussian AO basis sets. The statistical data for the deviations of computed sublimation energies from reference data are converted to normal error distributions shown in Figure 11. The plane-wave basis set PBE-D3 results are of high

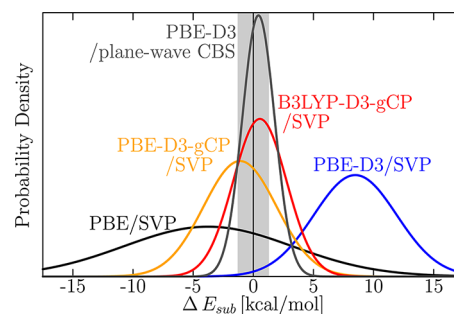


**Figure 11.** Deviations between experimental sublimation energies of the X23 set and theoretical calculations utilizing the PBE and B3LYP functional and small SVP basis set. The CBS values are estimated with a huge plane-wave basis set with an energy cutoff of 1000 eV. The statistical data are converted into normal error distributions. The gray shading denotes the experimental error interval. The quality of the theoretical methods is in the following (declining) order: PBE-D3/CBS, B3LYP-D3-gCP/SVP, PBE-D3-gCP/SVP, PBE-D3/SVP, and PBE/SVP.

quality, with a MAD below the estimated experimental uncertainty. From the small basis set calculations, PBE-D3-gCP/SVP and B3LYP-D3-gCP/SVP can also be recommended. The error spread at the PBE/SVP and PBE-D3/SVP levels is significant due to an incomplete account of dispersion and BSSE. This is also true for the B3LYP/SVP calculations if one of the corrections is neglected.

For the computation of the crystal structures at the SVP level, the BSSE seems to be overestimated by the counterpoise corrections. We suggest the following general strategy when small basis sets are employed. First, a geometry optimization using the atom pairwise dispersion correction D3 and 50% of the gCP correction (dubbed DFT-D3-(1/2)gCP) should be conducted. Subsequently, a single-point energy with two- and three-body dispersion energy and full counterpoise correction on the optimized structure (dubbed DFT-D3-gCP+E<sup>(3)</sup>) should be computed. If hydrogen bonds are present, the B3LYP functional is preferred over PBE. The gCP can be also

applied to denser systems, as demonstrated by the good results for the graphite stacking on the PBE-D3-gCP/SV level. The interlayer potential agrees remarkably well with BSSE-free plane-wave results on the PBE-D3/CBS level. The agreement with the experimental interlayer equilibrium interaction energy and distance is satisfactory.

We fitted the gCP parameters for a recently developed solid-state Gaussian basis set (pob-TZVP). For the adsorption of water on a nickel (110) surface as an example, the PBE-D3-gcp/pob-TZVP level was tested. For the Ni–O distance, a very good agreement with the experimental value was found.

The gCP method is implemented in a freely available FORTRAN program obtainable from the author's Web site and will be available in the next release of the CRYSTAL code. Similar to what has been pointed out recently for molecular thermochemistry,<sup>19</sup> it is recommended as a default for dispersion corrected, small basis set DFT or HF calculations also for solids.

## ■ ASSOCIATED CONTENT

### ● Supporting Information

Sublimation energies per molecule of all X23 organic crystals. Additional geometry information on the fully optimized structures. This material is available free of charge via the Internet at <http://pubs.acs.org>.

## ■ AUTHOR INFORMATION

### Corresponding Author

\*E-mail: [grimme@thch.uni-bonn.de](mailto:grimme@thch.uni-bonn.de).

### Present Address

<sup>†</sup>M.A.: Department of Chemistry, Humboldt University, Berlin, Germany.

### Notes

The authors declare no competing financial interest.

## ■ ACKNOWLEDGMENTS

This work is supported by Deutsche Forschungsgemeinschaft (DFG) under Grant SFB813 "Chemistry at Spin Centers — Concepts, Mechanisms, Functions".

## ■ REFERENCES

- (1) Sanderson, K. Model Predicts Structure of Crystals. *Nature* **2007**, *450*, 771.
- (2) Woodley, S. M.; Catlow, R. Crystal Structure Prediction from First Principles. *Nat. Mater.* **2008**, *7*, 937–946.
- (3) Neumann, M. A.; Leusen, F. J. J.; Kendrick, J. A Major Advance in Crystal Structure Prediction. *Angew. Chem., Int. Ed.* **2008**, *47*, 2427–2430.
- (4) Klimes, J.; Michaelides, A. Perspective: Advances and Challenges in Treating van der Waals Dispersion Forces in Density Functional Theory. *J. Chem. Phys.* **2012**, *137*, 120901.
- (5) Vydrov, O. A.; Van Voorhis, T. Nonlocal van der Waals Density Functional: The Simpler the Better. *J. Chem. Phys.* **2010**, *133*, 244103.
- (6) Civalieri, B.; Zicovich-Wilson, C. M.; Valenzano, L.; Ugliengo, P. B3LYP Augmented with an Empirical Dispersion Term (B3LYP-D\*) as Applied to Molecular Crystals. *CrystEngComm* **2008**, *10*, 405–410.
- (7) Jacobsen, H.; Cavallo, L. On the Accuracy of DFT Methods in Reproducing Ligand Substitution Energies for Transition Metal Complexes in Solution: The Role of Dispersive Interactions. *ChemPhysChem* **2012**, *13*, 562–569.
- (8) Burns, L. A.; Vazquez-Mayagoitia, A.; Sumpter, B. G.; Sherrill, C. D. A Comparison of Dispersion Corrections (DFT-D), Exchange-Hole Dipole Moment (XDM) Theory, and Specialized Functionals. *J. Chem. Phys.* **2011**, *134*, 084107.
- (9) Nanda, K.; Beran, G. Prediction of Organic Molecular Crystal Geometries from MP2-Level Fragment Quantum Mechanical/Molecular Mechanical Calculations. *J. Chem. Phys.* **2012**, *138*, 174106.
- (10) Wen, S.; Nanda, K.; Huang, Y.; Beran, G. Practical Quantum Mechanics-Based Fragment Methods for Predicting Molecular Crystal Properties. *Phys. Chem. Chem. Phys.* **2012**, *14*, 7578–7590.
- (11) Krukau, A. V.; Vydrov, O. A.; Izmaylov, A. F.; Scuseria, G. E. Influence of the Exchange Screening Parameter on the Performance of Screened Hybrid Functionals. *J. Chem. Phys.* **2006**, *125*, 224106.
- (12) Brandenburg, J. G.; Grimme, S.; Jones, P. G.; Markopoulos, G.; Hopf, H.; Cyranski, M. K.; Kuck, D. Unidirectional Molecular Stacking of Tribenzotriquinacenes in the Solid State — A Combined X-ray and Theoretical Study. *Chem.—Eur. J.* **2013**, *19*, 9930–9938.
- (13) Lippert, G.; Hutter, J.; Parrinello, M. A Hybrid Gaussian and Plane Wave Density Functional Scheme. *Mol. Phys.* **1997**, *92*, 477–488.
- (14) Lippert, G.; Hutter, J.; Parrinello, M. The Gaussian and Augmented-Plane-Wave Density Functional Method for Ab Initio Molecular Dynamics Simulations. *Theor. Chem. Acc.* **1999**, *103*, 124–140.
- (15) Pisani, C.; Dovesi, R.; Roetti, C. *Hartree–Fock Ab Initio Treatment of Crystalline Solids Lecture Notes in Chemistry Series*; Springer Verlag: Berlin, Germany, 1988; Vol. 48.
- (16) Dovesi, R.; Civalieri, B.; Orlando, R.; Roetti, C.; Saunders, V. *Ab Initio Quantum Simulation in Solid State Chemistry*; Wiley: New York, 2005; Vol. 21.
- (17) Gutowski, M.; Chalasiński, G. Critical Evaluation of Some Computational Approaches to the Problem of Basis Set Superposition Error. *J. Chem. Phys.* **1993**, *98*, 5540.
- (18) Kruse, H.; Grimme, S. A Geometrical Correction for the Inter- and Intra-molecular Basis Set Superposition Error in Hartree–Fock and Density Functional Theory Calculations for Large Systems. *J. Chem. Phys.* **2012**, *136*, 154101.
- (19) Kruse, H.; Goerigk, L.; Grimme, S. Why the Standard B3LYP/6-31G\* Model Chemistry Should Not Be Used in DFT Calculations of Molecular Thermochemistry: Understanding and Correcting the Problem. *J. Org. Chem.* **2012**, *77*, 10824–10834.
- (20) Grimme, S.; Antony, J.; Ehrlich, S.; Krieg, H. A Consistent and Accurate Ab Initio Parametrization of Density Functional Dispersion Correction (DFT-D) for the 94 Elements H–Pu. *J. Chem. Phys.* **2010**, *132*, 154104.
- (21) Otero-de-la Roza, A. O.; Johnson, E. R. A Benchmark for Non-covalent Interactions in Solids. *J. Chem. Phys.* **2012**, *137*, 054103.
- (22) Reilly, A. M.; Tkatchenko, A. Seamless and Accurate Modeling of Organic Molecular Materials. *J. Phys. Chem. Lett.* **2013**, *4*, 1028.
- (23) Reilly, A. M.; Tkatchenko, A. Understanding the Role of Vibration, Exact Exchange, and Many-Body van der Waals Interactions in the Cohesive Properties of Molecular Crystals. *J. Chem. Phys.* **2013**, *139*, 024705.
- (24) Ferrero, M.; Civalieri, B.; Rerat, M.; Orlando, R.; Dovesi, R. The Calculation of the Static First and Second Susceptibilities of Crystalline Urea: A Comparison of Hartree–Fock and Density Functional Theory Results Obtained with the Periodic Coupled Perturbed Hartree–Fock/Kohn–Sham Scheme. *J. Chem. Phys.* **2009**, *132*, 214704.
- (25) Maschio, L.; Usvyat, D.; Schütz, M.; Civalieri, B. Periodic Local Moeller–Plesset Second Order Perturbation Theory Method Applied to Molecular Crystals: Study of Solid NH<sub>3</sub> and CO<sub>2</sub> Using Extended Basis Sets. *J. Chem. Phys.* **2010**, *132*, 134706.
- (26) Maschio, L.; Usvyat, D.; Civalieri, B. Ab Initio Study of van der Waals and Hydrogen-Bonded Molecular Crystals with a Periodic Local-MP2 Method. *CrystEngComm* **2010**, *12*, 2429–2435.
- (27) Peintinger, M. F.; Oliveira, D. V.; Bredow, T. Consistent Gaussian Basis Sets of Triple-Zeta Valence with Polarization Quality for Solid-State Calculations. *J. Comput. Chem.* **2013**, *34*, 451–459.
- (28) Grimme, S. Density Functional Theory with London Dispersion Corrections. *WIREs Comput. Mol. Sci.* **2011**, *1*, 211.

- (29) Grimme, S.; Ehrlich, S.; Goerigk, L. Effect of the Damping Function in Dispersion Corrected Density Functional Theory. *J. Comput. Chem.* **2011**, *32*, 1456–1465.
- (30) Becke, A. D.; Johnson, E. R. A Density-Functional Model of the Dispersion Interaction. *J. Chem. Phys.* **2005**, *123*, 154101.
- (31) Axilrod, B. M.; Teller, E. Interaction of the van der Waals Type Between Three Atoms. *J. Chem. Phys.* **1943**, *11*, 299–300.
- (32) Casimir, H. B. G.; Polder, D. The Influence of Retardation on the London–van der Waals Forces. *Phys. Rev.* **1948**, *73*, 360–372.
- (33) Goerigk, L.; Kruse, H.; Grimme, S. Benchmarking Density Functional Methods against the S66 and S66 × 8 Datasets for Non-covalent Interactions. *ChemPhysChem* **2011**, *12*, 3421–3433.
- (34) Ehrlich, S.; Moellmann, J.; Grimme, S. Dispersion-Corrected Density Functional Theory for Aromatic Interactions in Complex Systems. *Acc. Chem. Res.* **2013**, *46*, 916–926.
- (35) Grimme, S. Supramolecular Binding Thermodynamics by Dispersion-Corrected Density Functional Theory. *Chem.—Eur. J.* **2012**, *18*, 9955.
- (36) Josaa, D.; Rodríguez-Otero, J.; Cabaleiro-Lagob, E. M.; Rellán-Piñeiro, M. Analysis of the Performance of DFT-D, M05-2X and M06-2X Functionals for Studying  $\pi$ - $\pi$  Interactions. *Chem. Phys. Lett.* **2013**, *557*, 170–175.
- (37) Chan, B.; Ball, G. E. A Benchmark Ab Initio and DFT Study of the Structure and Binding of Methane in the  $\sigma$  Alkane Complex  $\text{CpRe}(\text{CO})_2(\text{CH}_4)$ . *J. Chem. Theory Comput.* **2013**, *9*, 2199–2208.
- (38) Moellmann, J.; Grimme, S. Importance of London Dispersion Effects for the Packing of Molecular Crystals: A Case Study for Intramolecular Stacking in a Bis-thiophene Derivative. *Phys. Chem. Chem. Phys.* **2010**, *12*, 8500–8504.
- (39) Reckien, W.; Janetzko, F.; Peintinger, M. F.; Bredow, T. Implementation of Empirical Dispersion Corrections to Density Functional Theory for Periodic Systems. *J. Comput. Chem.* **2012**, *33*, 2023–2031.
- (40) Moellmann, J.; Ehrlich, S.; Tonner, R.; Grimme, S. A DFT-D Study of Structural and Energetic Properties of  $\text{TiO}_2$  Modifications. *J. Phys.: Condens. Matter* **2012**, *24*, 424206.
- (41) Sancho-García, J. C.; Aragón, J.; Ortí, E.; Olivier, Y. Obtaining the Lattice Energy of the Anthracene Crystal by Modern Yet Affordable First-Principles Methods. *J. Chem. Phys.* **2013**, *138*, 204304.
- (42) von Lilienfeld, O. A.; Tkatchenko, A. Two- and Three-Body Interatomic Dispersion Energy Contributions to Binding in Molecules and Solids. *J. Chem. Phys.* **2010**, *132*, 234109.
- (43) Tkatchenko, A.; DiStasio, R. A.; Car, R.; Scheffler, M. Accurate and Efficient Method for Many-Body van der Waals Interactions. *Phys. Rev. Lett.* **2012**, *108*, 236402.
- (44) Boys, S.; Bernardi, F. The Calculation of Small Molecular Interactions by the Differences of Separate Total Energies. Some Procedures with Reduced Errors. *Mol. Phys.* **1970**, *19*, 553–566.
- (45) Rezáč, J.; Riley, K. E.; Hobza, P. S66: A Well-balanced Database of Benchmark Interaction Energies Relevant to Biomolecular Structures. *J. Chem. Theory Comput.* **2011**, *7*, 2427.
- (46) Schäfer, A.; Horn, H.; Ahlrichs, R. Fully Optimized Contracted Gaussian Basis Sets for Atoms Li to Kr. *J. Chem. Phys.* **1992**, *97*, 2571–2577.
- (47) Schäfer, A.; Huber, C.; Ahlrichs, R. Fully Optimized Contracted Gaussian Basis Sets of Triple Zeta Valence Quality for Atoms Li to Kr. *J. Chem. Phys.* **1994**, *100*, 5829–5235.
- (48) Weigend, F.; Ahlrichs, R. Balanced Basis Sets of Split Valence, Triple Zeta Valence and Quadruple Zeta Valence Quality for H to Rn: Design and Assessment of Accuracy. *Phys. Chem. Chem. Phys.* **2005**, *7*, 3297–305.
- (49) Tatewaki, H.; Huzinaga, S. A Systematic Preparation of New Contracted Gaussian-Type Orbital Sets. III. Second-Row Atoms from Li through Ne. *J. Comput. Chem.* **1980**, *1*, 205–228.
- (50) Schuchardt, K. L.; Didier, B. T.; Elsethagen, T.; Sun, L.; Gurumoothi, V.; Chase, J.; Li, J.; Windus, T. L. Basis Set Exchange: A Community Database for Computational Sciences. *J. Chem. Inf. Model.* **2007**, *47*, 1045–1052.
- (51) Hehre, W. J.; Ditchfield, R.; Pople, J. A. Self-Consistent Molecular Orbital Methods. XII. Further Extensions of Gaussian-Type Basis Sets for Use in Molecular Orbital Studies of Organic Molecules. *J. Chem. Phys.* **1972**, *56*, 2257–2262.
- (52) Dovesi, R.; Orlando, R.; Civalleri, B.; Roetti, C.; Saunders, V. R.; Zicovich-Wilson, C. M. Z. *Kristallogr.* **2005**, *220*, 571.
- (53) Dovesi, R.; Saunders, V. R.; Roetti, C.; Orlando, R.; Zicovich-Wilson, C. M.; Pascale, F.; Civalleri, B.; Doll, K.; Harrison, N. M.; Bush, I. J.; et al. *CRYSTAL09 User's Manual*; University of Torino: Torino, Italy, 2009.
- (54) Perdew, J. P.; Burke, K.; Ernzerhof, M. Generalized Gradient Approximation Made Simple. *Phys. Rev. Lett.* **1996**, *77*, 3865–3868.
- (55) Perdew, J. P.; Burke, K.; Ernzerhof, M. Generalized Gradient Approximation Made Simple [Phys. Rev. Lett. *77*, 3865 (1996)]. *Phys. Rev. Lett.* **1997**, *78*, 1396–1396.
- (56) Becke, A. D. Density-Functional Thermochemistry. III. The Role of Exact Exchange. *J. Chem. Phys.* **1993**, *98*, 5648.
- (57) Stephens, P. J.; Devlin, F. J.; Chabalowski, C. F.; Frisch, M. J. Ab Initio Calculation of Vibrational Absorption and Circular Dichroism Spectra Using Density Functional Force Fields. *J. Phys. Chem.* **1994**, *98*, 11623.
- (58) Monkhorst, H. J.; Pack, J. D. Special Points for Brillouin-Zone Integrations. *Phys. Rev. B* **1976**, *13*, 5188–5192.
- (59) Kresse, G.; Furthmüller, J. Efficiency of Ab-Initio Total Energy Calculations for Metals and Semiconductors Using a Plane-Wave Basis Set. *Comput. Mater. Sci.* **1996**, *6*, 15–50.
- (60) Bucko, T.; Hafner, J.; Lebegue, S.; Angyan, J. G. Improved Description of the Structure of Molecular and Layered Crystals: Ab Initio DFT Calculations with van der Waals Corrections. *J. Phys. Chem. A* **2010**, *114*, 11814–11824.
- (61) Blöchl, P. E. Projector Augmented-Wave Method. *Phys. Rev. B* **1994**, *50*, 17953–17979.
- (62) Kresse, G.; Joubert, D. From Ultrasoft Pseudopotentials to the Projector Augmented-Wave Method. *Phys. Rev. B* **1999**, *59*, 1758–1775.
- (63) Grimme, S. *ANCOPT: Approximate Normal Coordinate Rational Function Optimization Program*; Universität Bonn: Bonn, Germany, 2013.
- (64) Eckert, F.; Pulay, P.; Werner, H.-J. Ab Initio Geometry Optimization for Large Molecules. *J. Comput. Chem.* **1997**, *18*, 1473–1483.
- (65) Thakkar, A. J.; Koga, T.; Saito, M.; Hoffmeyer, R. E. Double and Quadruple Zeta Contracted Gaussian Basis Sets for Hydrogen through Neon. *Int. J. Quantum Chem. Symp.* **1993**, *48*, 343.
- (66) Swaminathan, S.; Craven, B. M.; McMullan, R. K. The Crystal Structure and Molecular Thermal Motion of Urea at 12, 60 and 123 K from Neutron Diffraction. *Acta Crystallogr., Sect. B* **1984**, *40*, 300–306.
- (67) Chickos, J. S. Enthalpies of Sublimation after a Century of Measurement: A View as Seen through the Eyes of a Collector. *Netsu Sokutei* **2003**, *30*, 116.
- (68) Tkatchenko, A.; von Lilienfeld, O. A. Popular Kohn–Sham Density Functionals Strongly Overestimate Many-Body Interactions in van der Waals Systems. *Phys. Rev. B* **2008**, *78*, 045116.
- (69) Goerigk, L.; Grimme, S. A Thorough Benchmark of Density Functional Methods for General Main Group Thermochemistry, Kinetics, and Noncovalent Interactions. *Phys. Chem. Chem. Phys.* **2011**, *13*, 6670–6688.
- (70) Boese, R.; Weiß, H.-C.; Bläser, D. Die Schmelzpunktalternanz der kurzketigen n-Alkane: Einkristall-Röntgenstrukturanalysen von Propan bei 30 K und von n-Butan bis n-Nonan bei 90 K. *Angew. Chem.* **1999**, *111*, 1042–1045.
- (71) Risthaus, T.; Grimme, S. Benchmarking of London Dispersion-Accounting Density Functional Theory Methods on Very Large Molecular Complexes. *J. Chem. Theory Comput.* **2013**, *9*, 1580–1591.
- (72) Hyla-Kryspin, I.; Haufe, G.; Grimme, S. Weak Hydrogen Bridges: A Systematic Theoretical Study on the Nature and Strength of C–H...F–C Interactions. *Chem.—Eur. J.* **2004**, *10*, 3411–3422.
- (73) Karton, A.; Tarnopolsky, A.; Lamère, J.-F.; Schatz, G. C.; Martin, J. M. L. Highly Accurate First-Principles Benchmark Data Sets

for the Parametrization and Validation of Density Functional and Other Approximate Methods. Derivation of a Robust, Generally Applicable, Double-Hybrid Functional for Thermochemistry and Thermochemical Kinetics. *J. Phys. Chem. A* **2008**, *112*, 12868–12886.

(74) Zhao, Y.; Truhlar, D. G. Computational Characterization and Modeling of Buckyball Tweezers: Density Functional Study of Concave–Convex  $\pi\cdots\pi$  Interactions. *Phys. Chem. Chem. Phys.* **2008**, *10*, 2813–2818.

(75) Zhao, Y.; Schultz, N. E.; Truhlar, D. G. Design of Density Functionals by Combining the Method of Constraint Satisfaction with Parametrization for Thermochemistry, Thermochemical Kinetics, and Noncovalent Interactions. *J. Chem. Theory Comput.* **2006**, *2*, 364–382.

(76) Kim, K. S.; Tarakeshwar, P.; Lee, J. Y. Molecular Clusters of  $\pi$ -Systems: Theoretical Studies of Structures, Spectra, and Origin of Interaction Energies. *Chem. Rev.* **2000**, *100*, 4145–4186.

(77) Wu, J.; Pisula, W.; Müllen, K. Graphenes as Potential Material for Electronics. *Chem. Rev.* **2007**, *107*, 718–747.

(78) Girifalco, L. A.; Lad, R. A. Energy of Cohesion, Compressibility, and the Potential Energy Functions of the Graphite System. *J. Chem. Phys.* **1956**, *25*, 693–698.

(79) Trickey, S. B.; Müller-Plathe, F.; Diercksen, G. H. F. Interplanar Binding and Lattice Relaxation in a Graphite Dilayer. *Phys. Rev. B* **1992**, *45*, 4460–4468.

(80) Benedict, L. X.; Chopra, N. G.; Cohen, M. L.; Zettl, A.; Louie, S. G.; Crespi, V. H. Microscopic Determination of the Interlayer Binding Energy in Graphite. *Chem. Phys. Lett.* **1998**, *286*, 490–496.

(81) Zacharia, R.; Ulbricht, H.; Hertel, T. Interlayer Cohesive Energy of Graphite from Thermal Desorption of Polyaromatic Hydrocarbons. *Phys. Rev. B* **2004**, *69*, 155406–155413.

(82) Grimme, S.; Mück-Lichtenfeld, C.; Antony, J. Noncovalent Interactions between Graphene Sheets and in Multishell (Hyper)-Fullerenes. *J. Phys. Chem. C* **2007**, *111*, 11199.

(83) Grimme, S. Semiempirical GGA-Type Density Functional Constructed with a Long-Range Dispersion Correction. *J. Comput. Chem.* **2006**, *27*, 1787–1799.

(84) Dobson, J. F.; White, A.; Rubio, A. Asymptotics of the Dispersion Interaction: Analytic Benchmarks for van der Waals Energy Functionals. *Phys. Rev. Lett.* **2006**, *96*, 073201.

(85) Spanu, L.; Sorella, S.; Galli, G. Nature and Strength of Interlayer Binding in Graphite. *Phys. Rev. Lett.* **2009**, *103*, 196401.

(86) Ahlrichs, R.; Armbruster, M. K.; Bär, M.; Baron, H.-P.; Bauernschmitt, R.; Crawford, N.; Deglmann, P.; Ehrig, M.; Eichkorn, K.; Elliott, S.; et al. *TURBOMOLE 6.4*; Universität Karlsruhe: Germany, 2012. See also: <http://www.turbomole.com>.

(87) Henderson, M. A. The Interaction of Water with Solid Surfaces: Fundamental Aspects Revisited. *Surf. Sci. Rep.* **2002**, *46*, 1–308.

(88) Pangher, N.; Schmalz, A.; Haase, J. Structure Determination of Water Chemisorbed on Ni(110) by Use of X-ray Absorption Fine-Structure Measurements. *Chem. Phys. Lett.* **1994**, *221*, 189–193.

(89) Chichagov, A. V.; Varlamov, D. A.; Dilanyan, R. A.; Dokina, T. N.; Drozhzhina, N. A.; Samokhvalova, O. L.; Ushakovskaya, T. V. MINCRYST: A Crystallographic Database for Minerals, Local and Network (WWW) Versions. *Crystallogr. Rep.* **2001**, *46*, 876–879.